45th AIAA Aerospace Sciences Meeting and Exhibit
8 - 11 January 2007, Reno, Nevada

AIAA 2007-483

Aerodynamic Performance of a Corrugated Dragonfly Airfoil Compared with Smooth Airfoils at Low Reynolds Numbers

Masatoshi Tamai[1], Zhijian Wang[2], Ganesh Rajagopalan[3], Hui Hu[4](✉)
Iowa State University, Ames, Iowa, 50011

and

Guowei He[5]
LNM, Institute of Mechanics, Chinese Academy of Sciences, Beijing, 100080, P. R. China

An experimental study was conducted to investigate the flow behavior around a corrugated dragonfly airfoil compared with a traditional, streamlined airfoil and a flat plate. The experimental study was conducted at the chord Reynolds number of Re_C =34,000, i.e., the regime where Micro-Air-Vehicles (MAV) usually operate, to explore the potential applications of such bio-inspired airfoils for MAV designs. The measurement results demonstrated clearly that the corrugated dragonfly airfoil has much better performance over the streamlined airfoil and the flat plate in preventing large-scale flow separation and airfoil stall at the test low Reynolds number level. The detailed PIV measurements near the noses of the airfoils elucidated underlying physics about why the corrugated dragonfly airfoil could suppress flow separation and airfoil stall at low Reynolds numbers: Instead of having laminar separation, the protruding corners of the corrugated dragonfly airfoil were found to be acting as "turbulators" to generate unsteady vortices to promote the transition of the boundary layer from laminar to turbulent rapidly. The unsteady vortex structures trapped in the valleys of the corrugated cross section could pump high-speed fluid from outside to near wall regions to provide sufficient energy for the boundary layer to overcome the adverse pressure gradient, thus, discourage flow separations and airfoil stall.

Nomenclature

AOA	=	angle of attack
C	=	chord length of airfoils
Re_C	=	chord Reynolds number
N	=	total number of the frames of instantaneous PIV measurements
TKE	=	normalized turbulent kinetic energy, $TKE = \frac{1}{2}\rho(\overline{u'}^2 + \overline{v'}^2)/(\frac{1}{2}\rho U_\infty{}^2)$
u_i, v_i	=	instantaneous velocity components in *x, y* directions
U, V	=	mean velocity components in *x, y* directions, $U = \sum_{i=1}^{N} u_i / N$, $V = \sum_{i=1}^{N} v_i / N$ c
$\overline{u'}, \overline{v'}$	=	turbulent velocity fluctuations, $\overline{u'} = \sqrt{\sum_{i=1}^{N}(u_i - U)^2 / N}$, $\overline{v'} = \sqrt{\sum_{i=1}^{N}(v_i - V)^2}$
U_∞	=	wind tunnel operating velocity
ϖ_z	=	Spanwise voriticity, $\varpi_z = \frac{\partial v_i}{\partial x} - \frac{\partial u_i}{\partial y}$

[1] Graduate Student, Department of Aerospace Engineering.
[2] Associate Professor, Department of Aerospace Engineering, and AIAA Associate Fellow.
[3] Professor, Department of Aerospace Engineering, and AIAA Associate Fellow.
[4] Assistant Professor, Department of Aerospace Engineering, and AIAA Senior Member, email: huhui@iastate.edu.
[5] Professor and Director, the Laboratory for Nonlinear Mechanics.

I. Introduction

MICRO-Air-Vehicles (MAVs), which typically refer to palm-sized aircraft (e.g. with a maximum dimension about 10cm and a flight speed about 10m/s), are of great interest to both military and civilian applications. Equipped with video cameras, transmitters or sensors, these miniaturized aerial vehicles can perform surveillance, reconnaissance, targeting, or bio-chemical sensing tasks at remote, hazardous or dangerous locations. A concerted effort supported by the Defense Advanced Research Projects Agency (DARPA) in recent years has resulted in advancements in miniaturized digital electronics, micro fabrication, miniaturized power cells, remote communication, imaging and control devices and other enabling technologies. Such advances have turned the concept of MAVs as rapidly deployable eyes-in-the-sky from fiction into demonstrated facts. The continuing demand for such small and robust miniaturized aerial vehicles is making MAVs an emerging sector of the aerospace market, and MAVs are expected to become commonplace in the next ten to twenty years.

Although a number of MAVs, either in fixed wing or flapping wing designs, have already been developed by several universities, commercial, and government-funded endeavors, the airfoil and wing planform designs of the MAVs rely mainly on scaled-down versions of those used by convectional, "macro-scale" aircraft. Chord Reynolds number (Re_C), which is based on airfoil chord length and flight velocity, is used to characterize the aerodynamic performance of an airfoil. While traditional, "macro-scale" aircraft have a chord Reynolds number of about $10^6 \sim 10^8$, the chord Reynolds numbers of MAVs are usually in the range of $10^4 \sim 10^5$. The aerodynamic design principles applicable to traditional, "macro-scale" aircraft may not be used for MAVs anymore due to the significant difference in chord Reynolds numbers. As a result, airfoil shape and wing planform designs that are optimized for traditional, "macro-scale" aircraft are found to degrade significantly when used for MAVs [1]. Therefore, it is very necessary and important to establish novel airfoil shape and wing planform design paradigms for MAVs in order to achieve good aerodynamic performances as well as their flight agility and versatility.

A number of insects including locusts, dragonflies, and damselflies employ wings that are not smooth or simple cambered surfaces. The cross-sections of the wings have well-defined corrugated configurations (Fig. 1). Such corrugated design was found to be of great importance to the stability of the ultra-light wings to handle the spanwise banding forces and mechanical wear that the wing experiences during flapping [2, 3]. The corrugated wing design does not appear to be very suitable for flight since it would have very poor aerodynamic performance (i.e. low lift and extremely high drag) according to traditional airfoil design principles. However, several studies on dragonfly wings in steady flow or gliding flight [4-7] have led to surprising conclusions: a corrugated dragonfly wing could have better aerodynamic performances (i. e., higher lift and bigger lift-to-drag ratio) compared with conventional streamlined airfoils in the low Reynolds number regime where dragonflies usually fly.

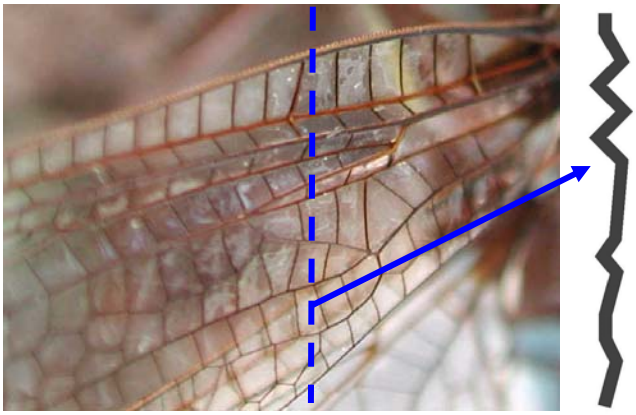

Figure 1. Corrugated cross section of a dragonfly wing

A number of hypotheses have been suggested to explain the fundamental mechanism of the rather unexpected aerodynamics performance improvement of the corrugated dragonfly airfoils or wings over conventional smooth airfoils. Rees [4] suggested that airflow could be trapped in the valleys of the corrugated structures to become stagnant or rotate slowly in the valleys, which resulting in the corrugated wing acting as a streamlined airfoil. Newman et al. [5] suggested that the improved aerodynamics performance would be associated with the earlier reattachment of the flow separation on the corrugated wings. As the angle of attack increases, airflow would separate from the leading edge to form a separation bubble, and the separated flow would reattach sooner due to the corrugation compared with smooth airfoils. Despite different explanations about the fundamental mechanism for the improved aerodynamics performance, most of the studies agree that corrugated dragonfly airfoils or wings work well in low Reynolds number regime, which naturally point to the potential applications of employing such bio-inspired airfoils or wings in micro-air-vehicles.

Most of the earlier experimental studies were conducted mainly based on the measurements of total aerodynamic forces (lift and drag) of either natural dragonfly wings or modeled corrugated wing sections. More recently, Kesel [8] conducted pressure measurements on the surfaces of a dragonfly wing model in addition to total lift and drag force measurements. Kesel [8] found that negative pressure would be produced at the valleys of the corrugated dragonfly wing model, which would contribute to the increased lift. Vargas and Mittal [9] conducted a numerical study on the flow around a 2-D dragonfly model to investigate the flow behaviors around the corrugated dragonfly airfoil. Their simulation results confirmed the existence of small vortex structures in the valleys of the corrugated dragonfly airfoil. The small vortex structures in the valleys of the corrugated cross section were also revealed qualitatively in the flow visualization of Kwok and Mittal [10].

Although several experimental studies have been conducted previously to investigate the aerodynamic performance of corrugated dragonfly airfoils or wings, detailed, quantitative flow measurements have never been made to elucidate the underlying physics of why corrugated dragonfly airfoils or wings could have superb aerodynamic performance for low Reynolds number flight. In this study, we report a detailed experimental investigation of the flow behavior around a modeled corrugated dragonfly airfoil, compared with a conventional, streamlined airfoil and a flat plate, at low Reynolds number. The experimental study was conducted in a wind tunnel with Particle Image Velocimetry (PIV) to make flow velocity field measurements. It should be noted that most previous studies on dragonfly wings or modeled dragonfly airfoils were conducted from a biologist point of view to investigate the flight aerodynamics of dragonflies. Thus, the chord Reynolds numbers are usually relatively small, i.e., $Re_C < 5{,}000$. With potential applications for MAVs in mind, we chose to conduct the present study at chord Reynolds number of $Re_C = 34{,}000$, i.e., in the range where MAVs usually operate.

II. Experimental Setup and Studied Airfoils

The experiments were performed in a closed-circuit low-speed wind tunnel located in the Aerospace Engineering Department of Iowa State University. The tunnel has a test section with a 1 × 1 ft (30 × 30 cm) cross section and all the walls of the test section optically transparent. The tunnel has a contraction section upstream the test section with honeycomb, screen structures and cooling system installed ahead of the contraction section to provide uniform low turbulent incoming flow to enter the test section.

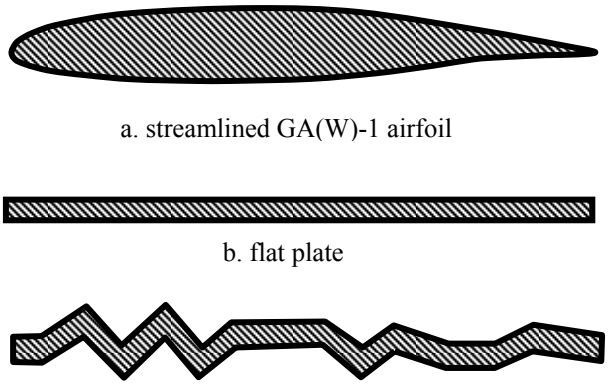

a. streamlined GA(W)-1 airfoil

b. flat plate

c. corrugated dragonfly airfoil

Figure 2. The test airfoils

Figure 2 shows the three airfoils used in the present study: a streamlined airfoil GA (W)-1 (also labeled as NASA LS(1)-0417) airfoil, a flat plate airfoil and a corrugated dragonfly airfoil. Compared with standard NACA airfoils, the GA (W)-1 airfoil was specially designed for low-speed aviation applications with a large leading-edge radius in order to flatten the peak in pressure coefficient near the airfoil nose to discourage flow separation [11]. The GA (W)-1 airfoil has the maximum thickness of 17% of the chord length. The flat plate has a rectangular cross section without any rounded treatment at the leading edge and trailing edge. The shape of the corrugated dragonfly airfoil corresponds to the forewing of a dragonfly (*Aeshna cyanea*) acquired at the mid section of the wing, which was digitally extracted from the profiles given in Kesel [8]. The flat plate and the corrugated dragonfly airfoil are made of wood plates with thickness of 4.0 mm. The flat plate airfoil, corrugated dragonfly airfoil and the streamlined GA (W)-1 airfoil have the same chord length, i. e., C = 101mm. The flow velocity at the inlet of the test section was set as $U_\infty = 5.0\,\text{m/s}$ for the present study, which corresponds to a chord Reynolds number of $\text{Re}_c = 3.4 \times 10^4$.

Figure 3 shows the experimental setup used in the present study. During the experiment, the test airfoils were installed in the middle of the test section. A PIV system was used to make flow velocity field measurements along the chord at the middle span of the airfoils. The flow was seeded with 1~5μm oil droplets. Illumination was

provided by a double-pulsed Nd:YAG laser (NewWave Gemini 200) adjusted on the second harmonic and emitting two pulses of 200 mJ at the wavelength of 532 nm with a repetition rate of 10 Hz. The laser beam was shaped to a sheet by a set of mirrors, spherical and cylindrical lenses. The thickness of the laser sheet in the measurement region is about 0.5mm. A high resolution 12-bit (1376 x 1040 pixel) CCD camera (SensiCam-QE, CookeCorp) was used for PIV image acquisition with the axis of the camera perpendicular to the laser sheet. The CCD cameras and the double-pulsed Nd:YAG lasers were connected to a workstation (host computer) via a Digital Delay Generator (Berkeley Nucleonics, Model 565), which controlled the timing of the laser illumination and the image acquisition.

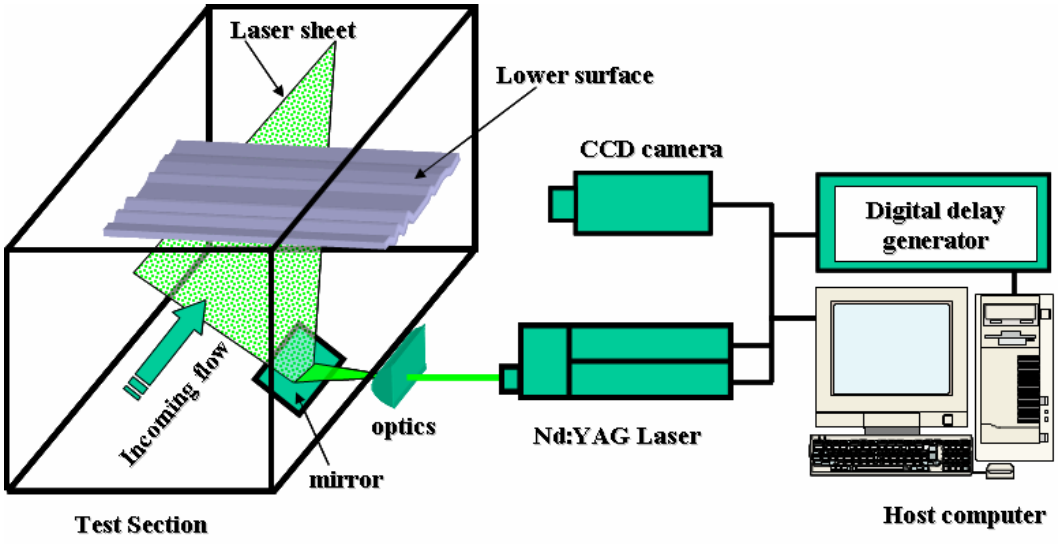

Figure 3. Experimental set up

Instantaneous PIV velocity vectors were obtained by a frame to frame cross-correlation technique involving successive frames of patterns of particle images in an interrogation window 32×32 pixels. An effective overlap of 50% was employed to satisfy the Nyquist criterion. The PIV measurements were conducted at two spatial resolutions: a coarse level to study the global features of the flows about the airfoils with the measurement window size of about 200mm×160mm; and a finer level to investigate the detailed flow structures near the nose of the airfoils with the measurement window size of about 50mm×40mm. The effective resolutions of the PIV measurements, i.e., grid sizes, were Δ/C = 0.048, and 0.012, respectively. After the instantaneous velocity vectors (u_i, v_i) were determined, spanwise vorticity (ϖ_z) could be derived. The time-averaged quantities such as mean velocity (U, V), turbulent velocity fluctuations ($\overline{u'}$, $\overline{v'}$) and normalized turbulent kinetic energy (TKE) distributions were obtained from a cinema sequence of 280 frames of instantaneous velocity fields. The measurement uncertainty level for the velocity vectors is estimated to be within 2.0%, and that of the turbulent velocity fluctuations ($\overline{u'}, \overline{v'}$) and turbulent kinetics energy (TKE) are about 5.0%. The uncertainty level of the spanwise vorticity data is expected to be within 10.0%.

III. Experimental Results and Discussions

Figure 4 shows the measured velocity fields around the airfoils at 5.0 degrees angle of attack. Even though the GA(W)-1 airfoil was specially designed to have a large leading-edge radius to flatten the peak in pressure coefficient near the airfoil nose to discourage flow separation, flow separation was still found to take place on the lifting surface even when the angle of attack was only 5 degrees because of the low Reynolds number. A large circulation bubble was generated near the trailing edge of the airfoil as a result of the flow separation. For the flat plate, the flow was found to attach to the upper surface of the flat plate, and no flow separation was found at 5.0 degrees angle of attack. For the corrugated dragonfly airfoil, while small circulation bubbles (zoom-in view is given in Fig. 9) were found to sit in the valleys of the corrugated cross section, high-speed streams outside the valleys were found to flow

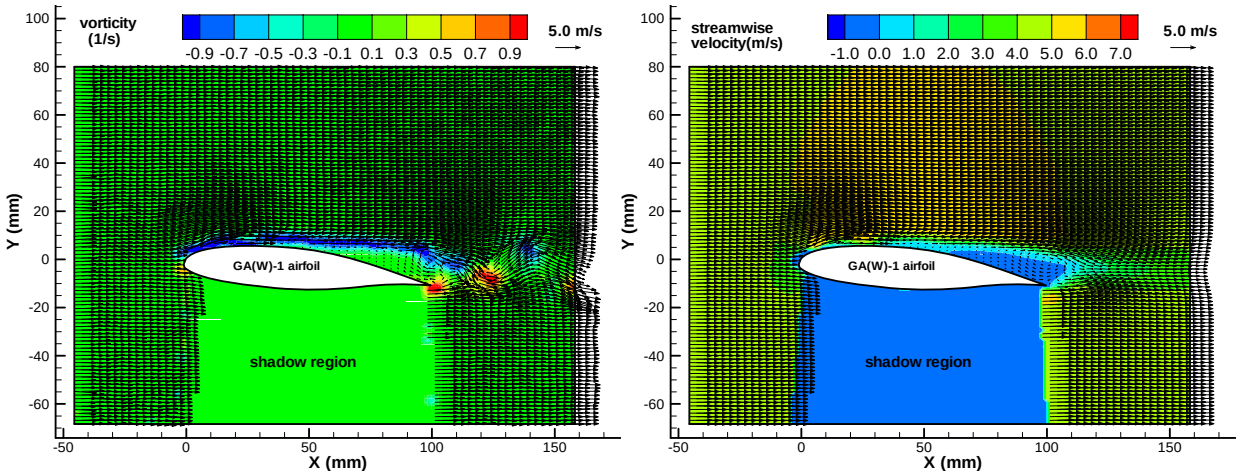

a. Instantaneous velocity field b. Ensemble-averaged velocity field

A. streamlined airfoil

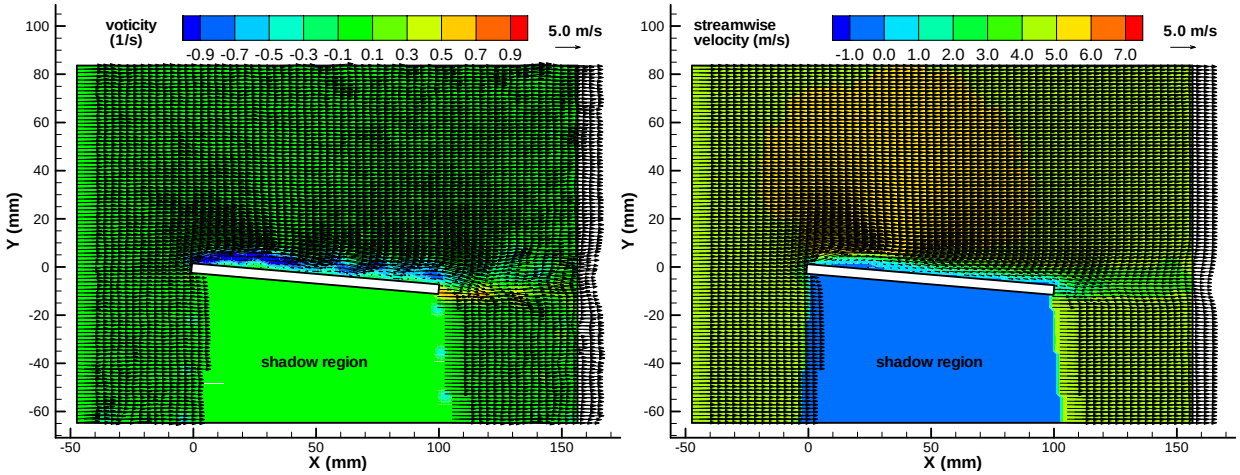

a. Instantaneous velocity field b. Ensemble-averaged velocity field

B. flat plate

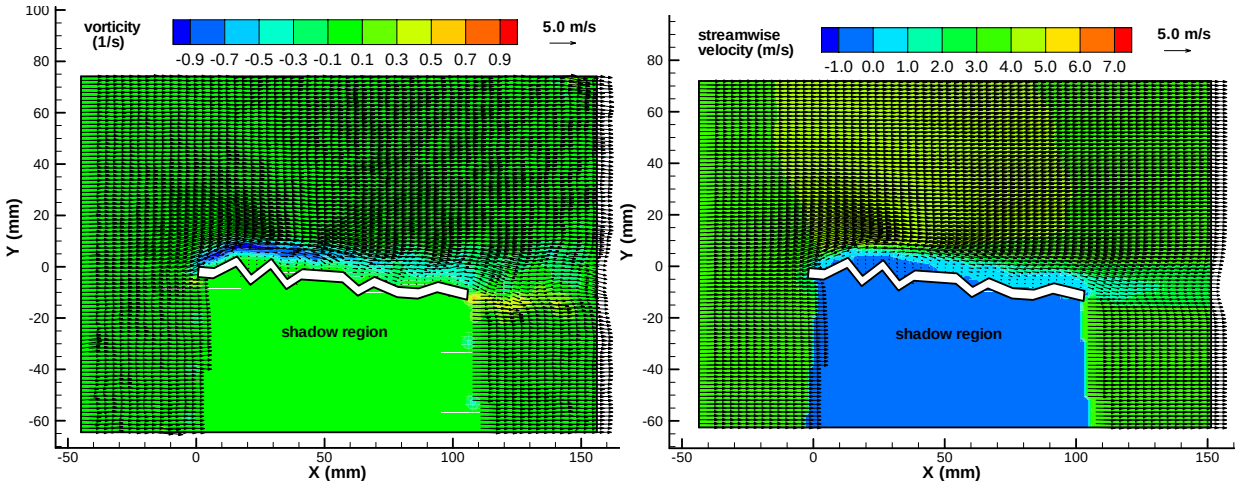

a. Instantaneous velocity field b. Ensemble-averaged velocity field

C. Corrugated dragonfly airfoil

Figure 4. PIV measurement results with AOA=5.0 (Re=34,000)

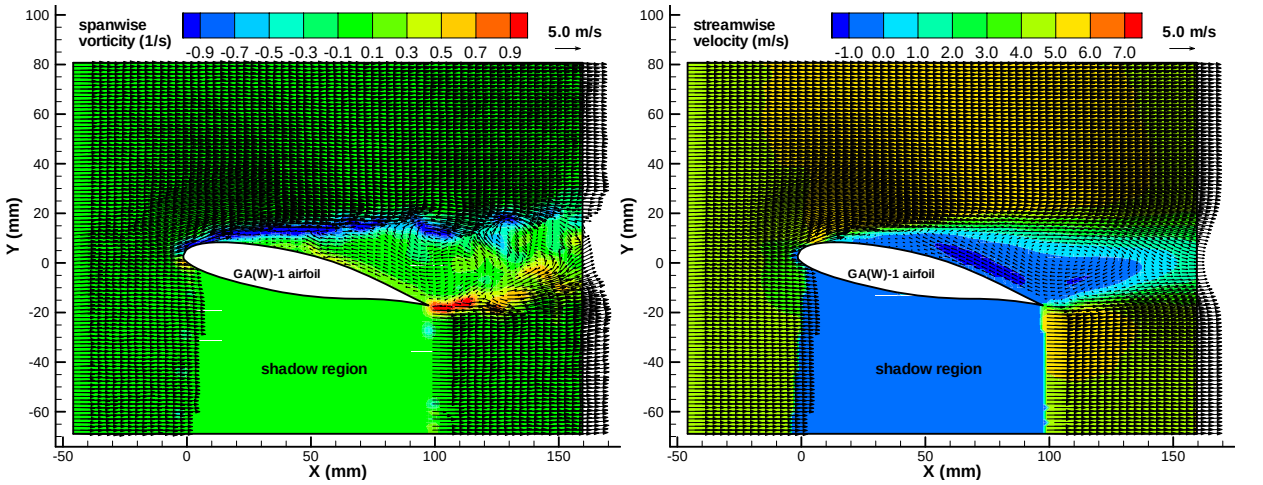

a. Instantaneous velocity field b. Ensemble-averaged velocity field

A. streamlined airfoil

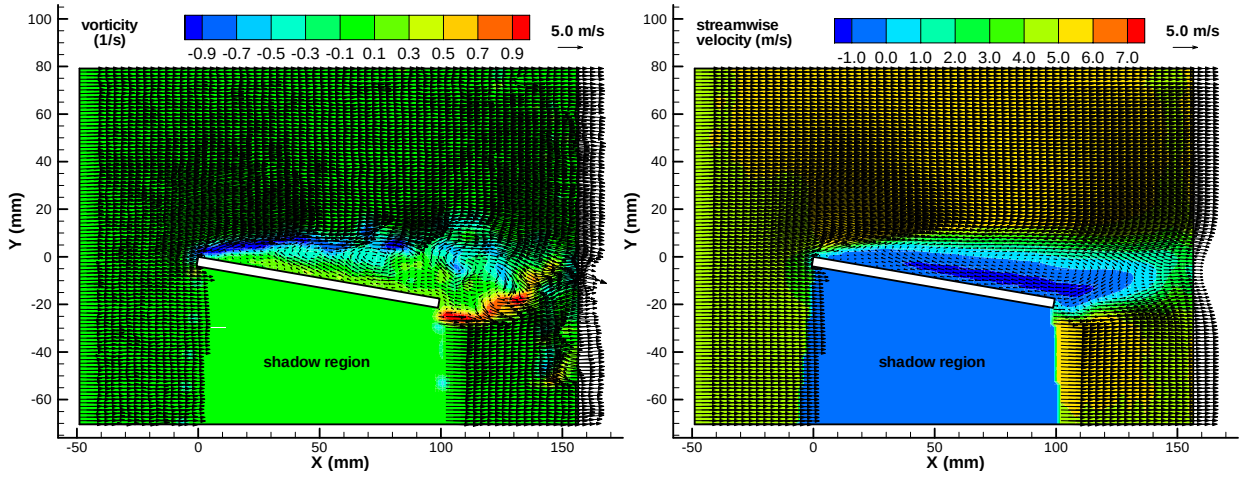

a. Instantaneous velocity field b. Ensemble-averaged velocity field

B. flat plate

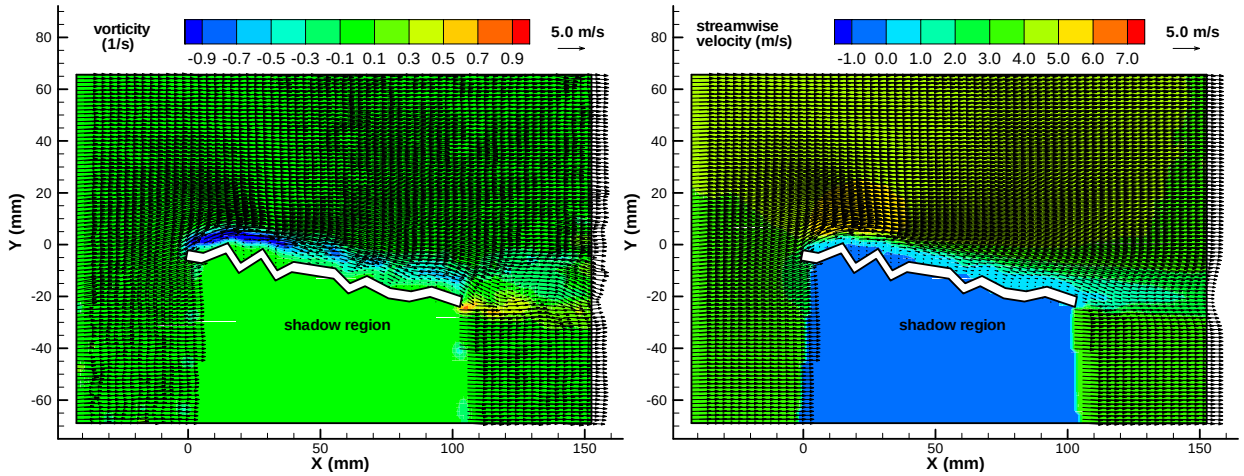

a. Instantaneous velocity field b. Ensemble-averaged velocity field

C. Corrugated dragonfly airfoil

Figure 5 PIV measurement results with AOA=10.0 (Re=34,000)

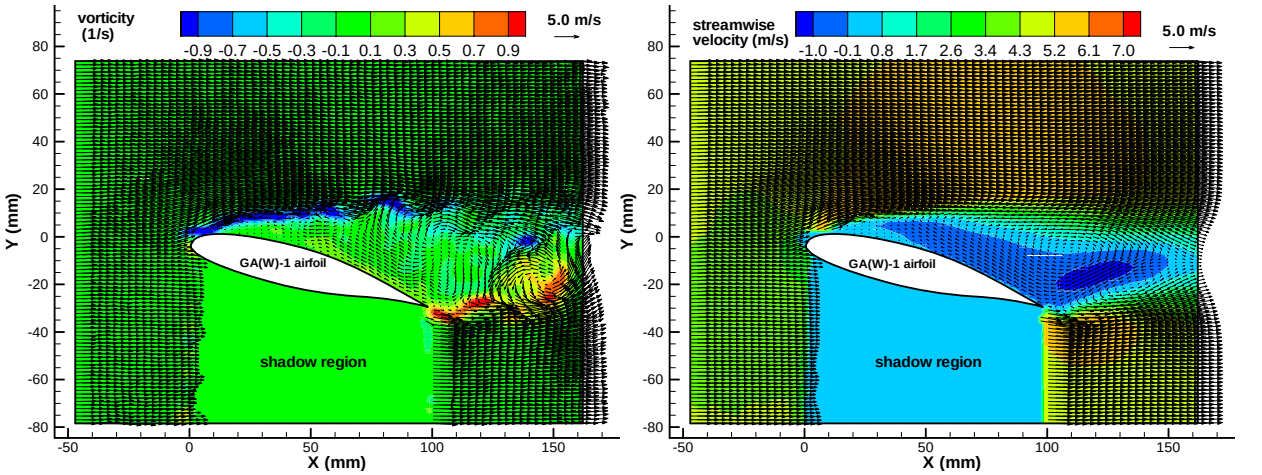

a. Instantaneous velocity field b. Ensemble-averaged velocity field

A. streamlined airfoil

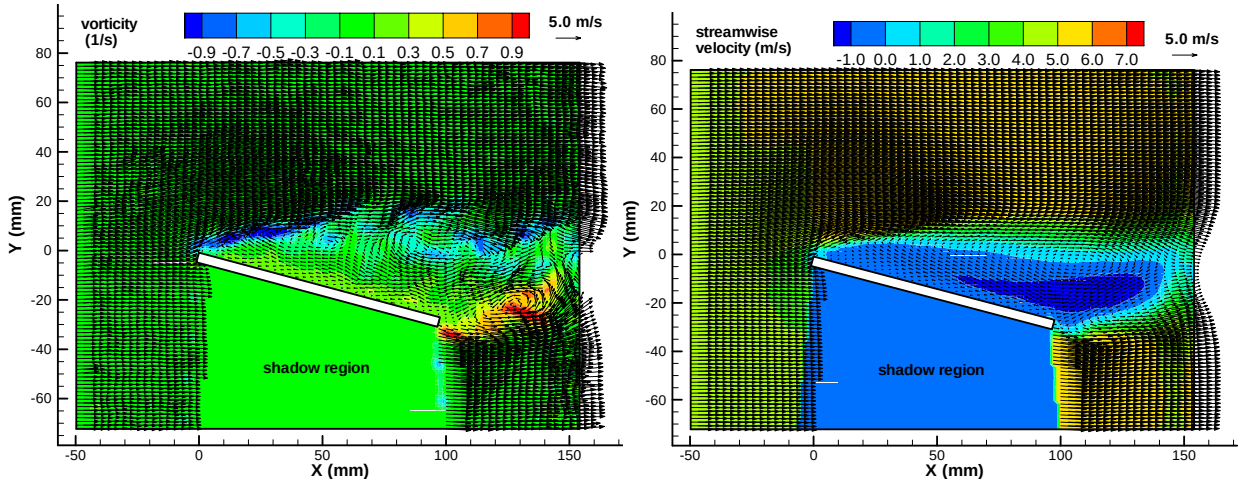

a. Instantaneous velocity field b. Ensemble-averaged velocity field

B. flat plate

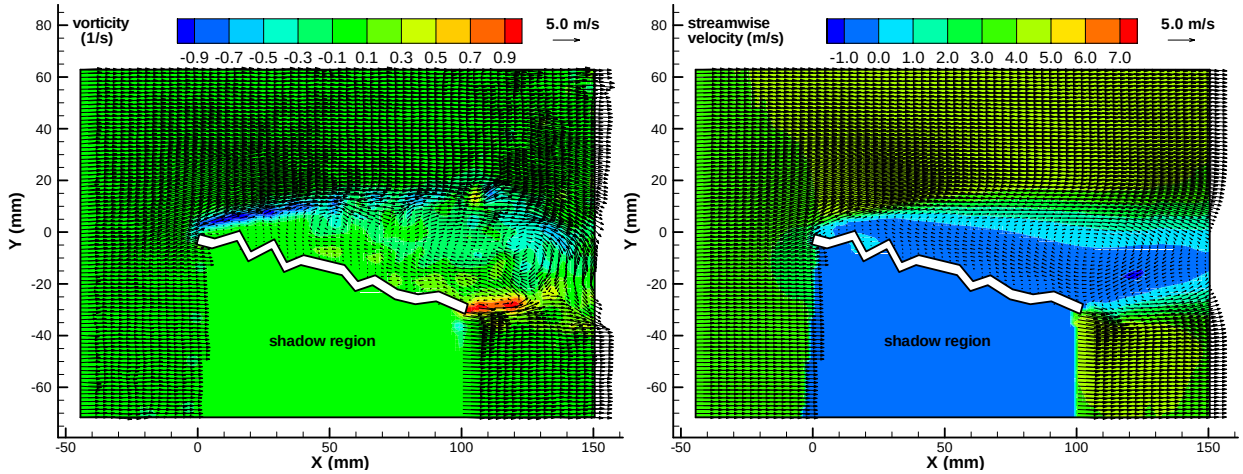

a. Instantaneous velocity field b. Ensemble-averaged velocity field

C. Corrugated dragonfly airfoil

Figure 6 PIV measurement results with AOA=15.0 (Re=34,000)

smoothly along an "envelope" profile constructed by fitting a spline through the protruding corners of the corrugated cross section (i.e., a smooth shape formed by filling the circulation bubbles solidly in the valleys). No large-scale flow separation could be found for the flow over the corrugated dragonfly airfoil at 5.0 degrees angle of attack.

Figure 6 shows the PIV measurement results when the angle of attack increased to 10 degrees. For the GA (W)-1 airfoil, the separation point, at where high-speed flow streams begin to separate from the upper surface of the streamlined GA (W)-1 airfoil, was found to move further upstream to approach airfoil leading edge compared with the case at 5 degrees angle of attack. The GA (W)-1 airfoil was found to stall completely, which resulted in a very large circulation region almost all over the lifting surface of the airfoil. The large deficit of the velocity profile at the exit of the measurement window (at about X=150mm) indicates a much big drag force acting on the GA (W)-1 airfoil due to the airfoil stall. As the angle of attack increased to 10 degrees, flow separation was also found on the upper surface of the flat plate due to the bigger adverse pressure gradient at larger angle of attack. The velocity deficit at the downstream of the flat plate was found to be smaller compared with that of the GA (W)-1 airfoil, which indicates a smaller drag. However, for the corrugated dragonfly airfoil, high-speed flow streams were still found to follow the "envelope" profile of the corrugated cross section faithfully, and no large-scale flow separation could be found over the corrugated dragonfly at 10.0 degrees angle of attack.

As angle of attack increasing, the adverse pressure gradient over the surface of the airfoils become bigger and bigger. Therefore, the separation regions over the upper surfaces of the GA (W)-1 airfoil and the flat plate enlarged significantly when the angle of attack increased to 15.0 degrees (Fig. 6). The velocity deficits downstream the GA (W)-1 airfoil and the flat plate at the exit of the measurement windows became much more serious compared with those with smaller angle of attack, which would indicate much large drag forces acting on the airfoils. Because of much larger adverse pressure gradient at 15.0 degrees angle of attack, the high-speed flow streams around the corrugated airfoil could not be able to follow the "envelope" profile of the corrugated cross section anymore. Large-scale flow separation was found to occur on the upper surface of the corrugated dragonfly airfoil, which resulted in a large circulation region downstream the corrugated dragonfly airfoil.

These PIV measurement results demonstrated clearly that the corrugated dragonfly airfoil could delay large-scale flow separation and airfoil stall to a much bigger angle of attack (up to about 12.5 degrees) compared with the streamlined GA-1(W) airfoil and the flat plate. However, it should also be noted that even though the corrugated dragonfly airfoil could delay the large-scale flow separation and airfoil stall, once flow separation were found to occur on the surface of the corrugated dragonfly airfoil, the circulation region downstream the corrugated dragonfly airfoil were found to be bigger than those downstream the streamlined GA-1(W) airfoil and the flat plate at the same angles of attack. The velocity deficit was also found to become much more serious at the exit of the measurement window, which indicates a bigger drag force acting on the airfoil.

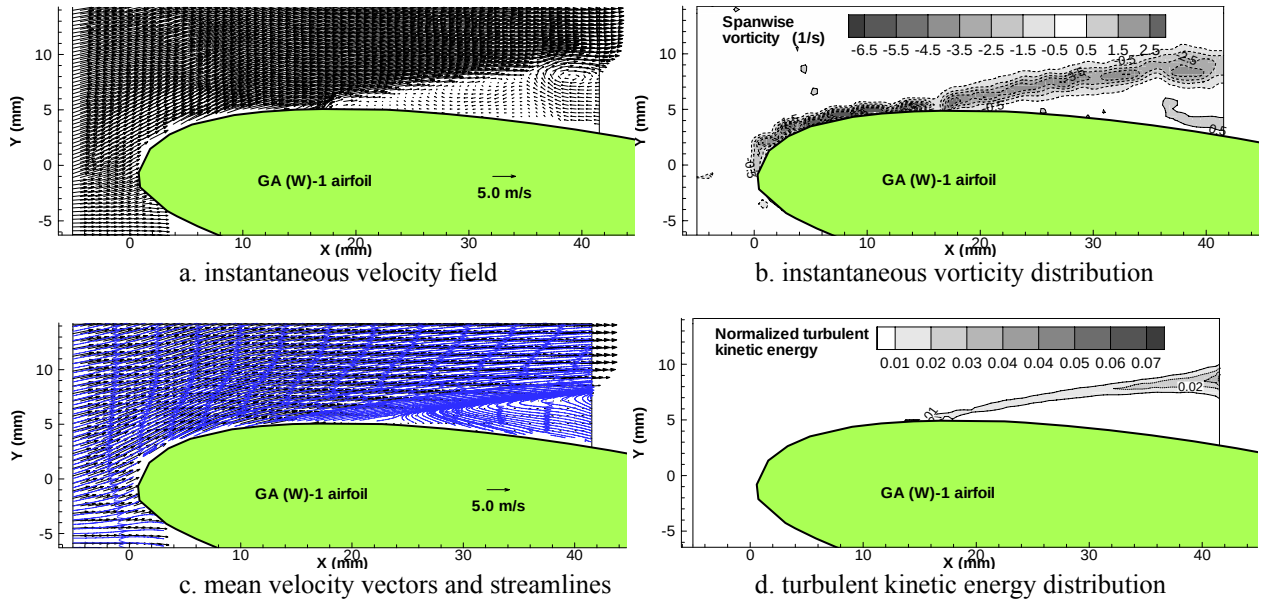

a. instantaneous velocity field

b. instantaneous vorticity distribution

c. mean velocity vectors and streamlines

d. turbulent kinetic energy distribution

Figure 7 PIV measurements around the nose of the streamlined airfoil at 10 degrees AOA.

In order to elucidate the fundamental mechanism why the corrugated dragonfly airfoil has a much better performance to prevent large-scale flow separation and airfoil stall compared with streamlined airfoils and flat plates at low Reynolds numbers, refined PIV measurements near the leading edges of the airfoils were made to investigate detailed flow structures around the noses of the airfoils. The measurement results were given in Fig. 7 to Fig. 9.

As described in the review articles of Lissaman [12] and Gad-el-Hak [13], for streamlined airfoils at low Reynolds numbers ($Re_C < 10^5$), the boundary layers would remain laminar at the onset of the pressure recovery unless artificially tripped. Laminar boundary layers are unable to withstand any significant adverse pressure gradient. Therefore, the performance of traditional, streamlined airfoils at low Reynolds numbers is entirely dictated by the relatively poor separation resistance of the laminar boundary layers. The laminar boundary layer over the streamlined GA (W)-1 airfoil was visualized clearly as a thin vortex layer over the nose of the airfoil in the instantaneous vorticity distribution given in Fig. 7. As indicated in the PIV measurements, the laminar boundary layer would separate easily from the upper surface of the streamlined airfoil since the laminar boundary layer has poor resistance to the adverse pressure gradient. As shown in the mean velocity field, a large-scale circulation bubble was generated over the upper surface of the GA (W)-1 airfoil after the separation point. The separated boundary layer behaved more like a free shear layer, which was highly unstable, therefore, rolling-up of Kelvin-Helmohtz vortex structures and transition to turbulence would be readily realized. Because of the laminar nature of the flow around the nose of the streamlined airfoil, the regions with higher turbulent kinetic energy were found to be confined within the thin shear layer after the laminar boundary layer separates from the upper surface of the GA (W)-1 airfoil.

Since a turbulent boundary layer is usually more capable (at least by a factor of 10) of advancing against adverse pressure gradient without flow separation [12], the necessity of eliminating laminar separation to improve aerodynamic performances of streamlined airfoils at low Reynolds numbers has led to the development of techniques to artificially accelerate transition, or to "turbulate" the laminar boundary layers over streamlined airfoils. A wide variety of transition-promoting devices, called "turbulators", has already been suggested to accomplish this and they are discussed in detail by Carmichael [14].

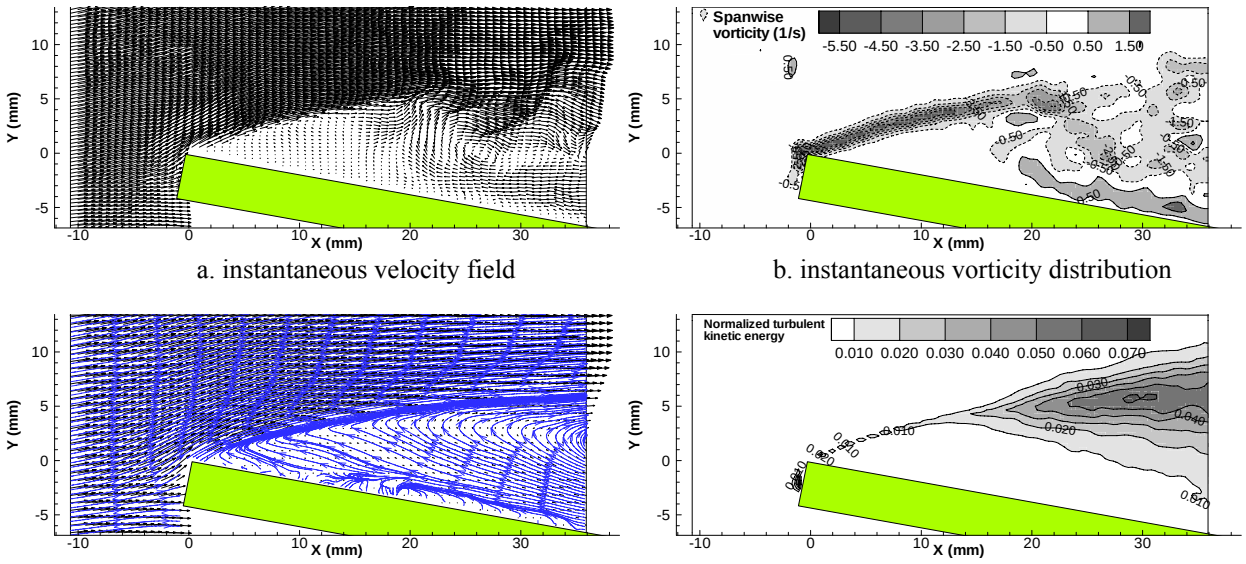

a. instantaneous velocity field

b. instantaneous vorticity distribution

c. mean velocity vectors and streamlines

d. turbulent kinetic energy distribution

Figure 8 PIV measurements around the nose of the flat plate at 10 degrees AOA.

Figure 8 reveals the flow behavior around the nose of the flat plate at 10 degrees angle of attack. High-speed fluid stream was found to separate from the upper surface of the flat plate right from the leading edge due to the low Reynolds number. The instantaneous velocity field and the instantaneous vorticity distribution show that the separated flow stream "taking off" at the leading edge of the flat plate formed a laminar shear layer at first, then, transited to be turbulent subsequently. Unsteady vortex structures were found to be generated after transition due to

the Kelvin-Helmholtz instabilities. Compared with those vortex structures near the nose of the streamlined GA (W)-1 airfoil, these unsteady vortex structures were found to be much stronger. The stronger vortex structures would enhance the mass and energy transfer between the high-speed fluid streams and the near wall circulating fluid, which resulted in a much higher turbulent kinetic energy level compared with that of the streamlined airfoil. Since the stronger Kelvin-Helmholtz vortex structures could entrain more high-speed fluid stream into the near wall region, therefore, the circulation bubble and the velocity deficit at the downstream of the flat plate would be smaller than those of the streamlined GA (W)-1 airfoil, as revealed clearly in the PIV measurement results given in Fig. 5.

Flow around the corrugated dragonfly airfoil is much more involved than those of the flat plate and the streamlined GA (W)-1 airfoil. As visualized in the PIV measurement results given in Fig. 9, unsteady vortices were found to shed periodically from the protruding corners of the corrugated cross section, and the laminar boundary layer starting from the leading edge was found to transit to turbulent rapidly as it approached the first protruding corner. The protruding corners of the corrugated dragonfly airfoil seem to act as "turbulators" to generate unsteady vortex structures that promote the transition of the boundary layer from laminar to turbulent. Unlike those found for the streamlined GA (W)-1 airfoil and flat plate where the turbulence transitions of the laminar boundary layers were found after the high-speed flow streams separated from the upper surfaces of the airfoils, the transition of the laminar boundary layer over the upper surface of the corrugated dragonfly airfoil was conducted without laminar flow separation. The unsteady vortex structures shedding from the protruding corners were found to be trapped in the valleys of the corrugated cross section, which would interact with the high-speed flow streams outside the valleys dynamically. Thanks to the interaction between the unsteady vortex structures and outside high-speed flow streams, high-speed fluid was pumped to near wall regions, which provided sufficient energy for the boundary layer to overcome the adverse pressure gradient to suppress flow separation and airfoil stall. The mean velocity vectors and streamlines revealed that small circulation bubbles would be formed to fill in the valleys of the corrugated dragonfly airfoil. High-speed streams outside the valleys would flow smoothly along the "envelope" profile of the corrugated cross section (i.e., the profile was formed as the valleys were solidly filled with the small circulation bubbles). The rapid transition of the boundary layer from laminar to turbulent could also be seen clearly from the turbulent kinetic energy (*TKE*) distribution, where the contour lines of the regions with higher turbulent kinetic energy were found to diverge rapidly at the first protruding corner of the corrugate dragonfly airfoil. The entrainment of high-speed fluid to near wall regions by the unsteady vortex structures resulted in much higher turbulent kinetic energy (*TKE*) level in the regions. Compared with the laminar boundary layer near the nose of the streamlined airfoil as shown in Fig. 7, such "energetic" turbulent boundary layer over the upper surface of the corrugated dragonfly airfoil would be much more capable of advancing against adverse pressure gradient to suppress flow separation. Therefore, high-speed flow streams would be able to attach to the "envelope" profile of the corrugated dragonfly airfoil faithfully even at much larger angle of attack, while the large-scale flow separation and airfoil stall had already been found for the flat plate and streamlined GA (W)-1 airfoil.

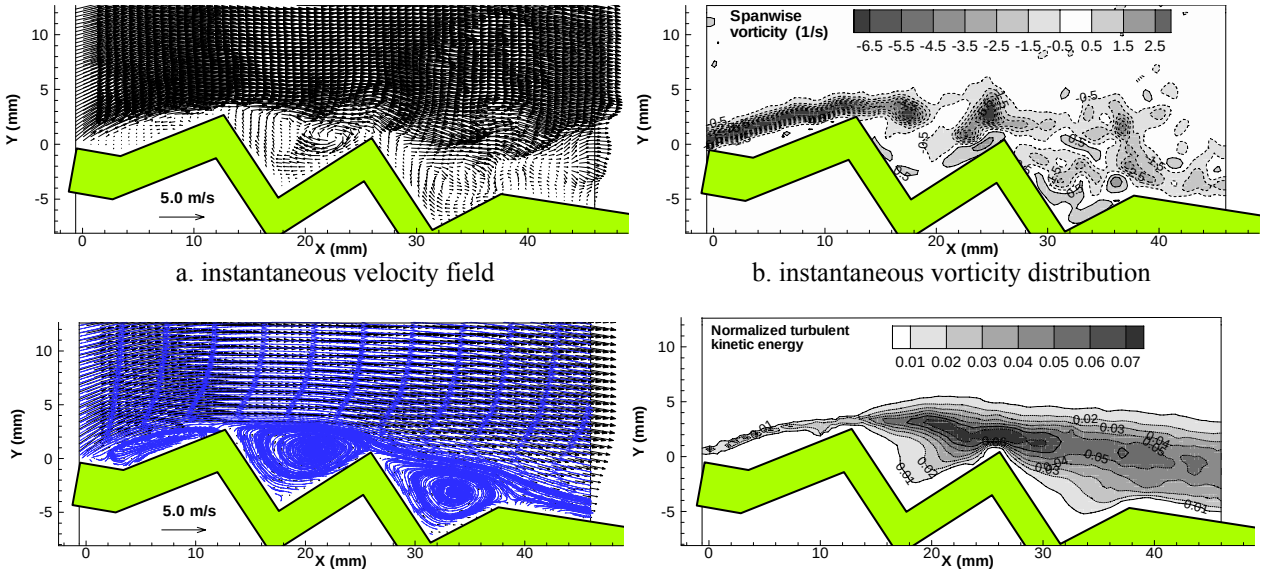

a. instantaneous velocity field

b. instantaneous vorticity distribution

c. mean velocity vectors and streamlines

d. turbulent kinetic energy distribution

Figure 9 PIV Measurements around the nose of the corrugated dragonfly airfoil at 10 degrees AOA.

IV. Concluding Remarks

An experimental study was conducted to investigate flow features around a corrugated dragonfly airfoil compared with a streamlined GA (W)-1 airfoil and a flat plate at low chord Reynolds number level of 34,000 to explore the potential applications of non-traditional, corrugated dragonfly airfoils for MAV designs. The measurement results demonstrated clearly that the corrugated dragonfly airfoil has much better performance over the streamlined airfoil and flat plate in preventing flow separation and airfoil stall at low Reynolds numbers. Because of the low Reynolds number, large-scale flow separation was already found on the upper surface of the streamlined airfoil when the angle of attack only at 5.0 degrees. Flow separation was also found on the upper surface of the flat plate as the angle of attack reaches 8 degrees. No apparent large-scale flow separation or airfoil stall could be found for the corrugated dragonfly airfoil until 12.5 degrees angle of attack. The detailed PIV measurements near the noses of the airfoils elucidated underlying physics about why the corrugated dragonfly airfoil could suppress large-scale flow separation and airfoil stall at low Reynolds numbers. Instead of having laminar separation, the protruding corners of the corrugated dragonfly airfoil were found to be acting as "turbulators" to generate unsteady vortices to promote the transition of the boundary layer from laminar to turbulent rapidly. The unsteady vortices trapped in the valleys of the corrugated cross section could pump high-speed fluid from outside to near wall regions to provide sufficient energy for the boundary layer flow to overcome the adverse pressure gradient, thus, discourage flow separations and airfoil stall. Although several pervious investigations have been conducted to study aerodynamics of dragonfly wings or/and corrugated dragonfly airfoils, the work reported at here is believed to be the first to provide detailed, quantitative flow measurements to elucidate the underlying physics of why corrugated dragonfly airfoils could have superb aerodynamic performance for low Reynolds number flight and to explore their potential applications in MAV designs.

Acknowledgments

The authors also want to thank Mr. Bill Rickard and Mr. Zifeng Yang of Iowa State University for their help in conducting the experiments. The support of National Science Foundation CAREER program to Hui Hu under award number of CTS-0545918 is gratefully acknowledged. Guowei He acknowledges the support from National Natural Science Foundation of China under the Project No.10325211.

.

References

[1] Mueller, T. J. (ed.), *Fixed and Flapping Wing Aerodynamics for Micro Air Vehicle Applications* (Progress in Astronautics and Aeronautics), ISBN 1-56347-517-0. 2001.

[2] Rees, C. J. C., "Form and function in corrugated insect wings," *Nature,* Vol. 256, 1975a, pp.200-203.

[3] Kesel, A. B., Philippi, U. and Nachtigall, W**.,** "Biomechanical Aspects of Insect Wings – An Analysis using the Finite Element Method," *Computers in Biology and Medicine,* Vol. 28, 1998, pp. 423–437.

[4] Rees, C. J. C**., "**Aerodynamic Properties of an Insect Wing Section and a Smooth Aerofoil Compared," *Nature*, Vol. 258, 13, Nov. 1975, pp141-142.

[5] Newman, B. G., Savage, S. B., and Schouella, D., "Model Test on a Wing Section of an *Aeschna* Dragonfly", *Scale Effects in An mal Locomotion,* edited by T. J. Pedley, London Academic Press, 1977, pp. 445-477.

[6] Okamoto, M., Yasuda, K., and Azuma, A., "Aerodynamic Characteristics of the Wings and Body of a Dragonfly." *Journal of Experimental Biology*. Vol. 199, 1996, pp. 281- 294.

[7] Wakeling, J. M. and Ellington, C. P**., "**Dragonfly flight I. Gliding Flight and Steady-state Aerodynamic Forces," *Journal of Experimental Biology*, Vol. 200, 1997, pp.543–556.

[8] Kesel, A. B., "Aerodynamic Characteristics of Dragonfly Wing Sections Compared with Technical Aerofoil," *Journal of Experimental Biology*, Vol. 203, 2000, pp. 3125-3135.

[9] Vargas, A. and Mittal, R. "Aerodynamic Performance of Biological Airfoils," AIAA 2004-2319, 2nd Flow Control Conference, Portland, Oregon, 2004.

[10] M. Kwok and R. Mittal, "Experimental Investigation of the Aerodynamics of a Modeled Dragonfly Wing Section" AIAA region I-MA Student Conference, Charlottesville, Virginia April 8-9, 2005.

[11] McGee, R.J. and Beasley W.D., "Low-speed Aerodynamics Characteristics of a 17-Percent-Thick Airfoil Section Designed for General Aviation Applications", NASA TN D-7428, 1973.

[12] Lissaman, P. B. S., "Low-Reynolds-Number Airfoils," *Annual Review of Fluid Mechanics*, Vol. 15, 1983, pp.223–239.

[13] Gad-el-Hak, M. "Micro-Air-Vehicles: Can They be Controlled Better," *Journal of Aircraft*, Vol. 38, No. 3, 2001, pp. 419-429.

[14] Carmichael, B. H., 1981, "Low Reynolds number airfoil Survey", Vol. 1, NASA CR-165803, 1981.